ChemComm

COMMUNICATION

View Article Online
View Journal | View Issue

Cite this: *Chem. Commun.*, 2014, **50**, 13081

Received 17th July 2014,
Accepted 3rd September 2014

DOI: 10.1039/c4cc05506c

www.rsc.org/chemcomm

A microporous six-fold interpenetrated hydrogen-bonded organic framework for highly selective separation of C_2H_4/C_2H_6†

Peng Li,[a] Yabing He,[a] Hadi D. Arman,[a] Rajamani Krishna,[b] Hailong Wang,[a] Linhong Weng[c] and Banglin Chen*[ad]

A unique six-fold interpenetrated hydrogen-bonded organic framework (HOF) has been developed, for the first time, for highly selective separation of C_2H_4/C_2H_6 at room temperature and normal pressure.

As one of the most important petrochemicals, ethylene is used widely in the chemical industry and its worldwide production exceeds that of any other organic compound (140 million tons per year by 2010).[1] Thermal cracking of ethane as a feedstock in the presence of steam remains one of the most important and widely employed processes for ethylene production. Due to the similar sizes and volatilities of ethylene and ethane, the traditional cryogenic distillation technology to separate ethylene from ethane requires distillation columns with over 100 trays under the conditions of high pressure (23 bar) and low temperature (−25 °C), which has been criticized as the most energy extensive process in the petrochemical industry.[2] Therefore, tremendous efforts have been devoted to develop alternative technologies,[3] such as membrane separation,[4] liquid adsorbent separation[5] and solid adsorbent adsorption separation[6] for ethylene/ethane separation at ambient temperature and pressure with lower energy cost.

In the development of adsorption separation technologies, various porous materials, such as SiO_2,[7] zeolites,[8] molecular sieves,[9] metal–organic frameworks (MOFs),[10] nanoparticle–MOF composites,[11] porous organic polymers (POPs),[12] activated carbons,[13] and carbon nanotubes,[14] have been explored as solid adsorbents to realize olefin/paraffin separation. Two useful but distinct strategies have been proposed to achieve preferential adsorption of olefin over paraffin. One is based on reversible formation of π-complexes of olefins with transition metal cations, and the other is control of the appropriate pore size and volume for size exclusion separation. The former strategy has been successfully applied in MOFs[10a] and POPs[12a] to realize high selective adsorption for ethylene over ethane. Although this selectivity is usually very high at low pressure, it decreased significantly with increasing pressure possibly due to saturation of the preferential binding sites. The latter strategy often used in propene/propane separation,[10b,12b] however, can hardly be achieved especially for smaller ethylene and ethane molecules with tiny dimensional difference. Moreover, this strategy may result in an inevitable low adsorption capacity.[10d] Hence, finding new materials for the adsorptive separation of ethylene–ethane mixtures is very challenging and important.

Recently, we and several other groups have discovered that hydrogen-bonded organic framework (HOF) materials can be used as a new class of porous materials for a variety of applications.[15] Because HOFs have some obvious advantages such as solvent processability and straightforward regeneration by recrystallization, while they might have different pore surfaces from those of well-established porous materials, exploration of HOF materials might lead to some unique new adsorbents for gas separations. Actually, the first HOF-1 exhibits superior performance to MOFs in very challenging C_2H_2/C_2H_4 separation.[15h] Herein, we report the synthesis of a robust hydrogen-bonded organic framework (**HOF-4**), which shows a high ideal adsorbed solution theory (IAST) selectivity of 14 for ethylene/ethane separation at room temperature and normal pressure.

The new tetrahedral molecular tecton **2** (Scheme 1) has been synthesized as a building block based on the following considerations: (i) extended tecton **2** has both tetrahedral symmetry and diaminopyridine in tecton **1**, which is the basic building unit of HOF-1 and is capable of forming multiple hydrogen bonds and thus extending into the 3D framework; (ii) generally speaking, longer ligands will lead to larger voids.

The tetrahedral organic building block **2** was readily synthesized in 92% yield by the reaction of the corresponding nitrile

[a] *Department of Chemistry, University of Texas at San Antonio, One UTSA Circle, San Antonio, Texas 78249-0698, USA. E-mail: banglin.chen@utsa.edu; Fax: +1-210-458-7428*
[b] *Van't Hoff Institute for Molecular Sciences, University of Amsterdam, Science Park 904, 1098 XH Amsterdam, The Netherlands*
[c] *Department of Chemistry, Fudan University, Shanghai, 200433, People's Republic of China*
[d] *Department of Chemistry, Faculty of Science, King Abdulaziz University, Jeddah 22254, Saudi Arabia*

† Electronic supplementary information (ESI) available: Synthesis and characterization of **HOF-4**, PXRD, TGA, FTIR spectra, sorption isotherms, and breakthrough simulations. CCDC 1010353. For ESI and crystallographic data in CIF or other electronic format see DOI: 10.1039/c4cc05506c

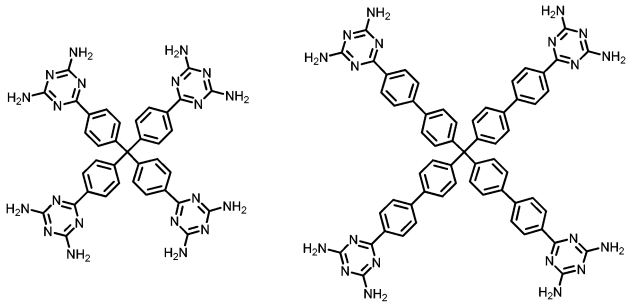

1 2

Scheme 1 Tetrahedral building blocks.

with dicyandiamide (see Scheme S1 in the ESI†). The colorless needle-like crystals of HOF-4 were easily isolated in 79% yield by evaporating DMF solution of **2** for a week at room temperature. The purity of **HOF-4** was confirmed by ^{1}H NMR and ^{13}C NMR spectroscopy, thermogravimetric analysis (TGA), and powder X-ray diffraction (PXRD) (Fig. S1–S3, ESI†). Single crystal X-ray diffraction reveals that **HOF-4** crystallizes in the monoclinic space group *P*2/*n* and shows a 3D architecture consisting of six equivalent interwoven nets of **PtS** topology.‡ For a single net, the asymmetric unit consists of only half of the building blocks (Fig. 1a left), and each building block is connected with six neighbouring ones by 12 strong hydrogen bonds involving the 2,4-diaminotriazine (DAT) groups (Fig. 1a right, the parameters of hydrogen bonding are listed in Table S1, ESI†). There exist rhombic channels in the single net along the [101] direction with an approximate dimension of 40 Å × 30 Å along the diagonals (Fig. S4, ESI†). If one considers the tetrahedral building block to be a four-connected node in the tetrahedral geometry, and the multiple hydrogen bonding motif of DAT groups to be a four-connected node in the square planar geometry, the single net of **HOF-4** can then be rationalized as a 3D **PtS** $\{4^2 8^4\}$ network topology (Fig. 1b). Due to large void spaces, six equivalent nets interpenetrate each other *via* intermolecular π···π interactions between the benzene rings (Fig. 1c). This high fold net interpenetration is expected to enhance the framework stability.[16–18] The rhombic channels along the [101] direction are completely blocked due to the interpenetration, leaving a 1D rectangular channel (3.8 Å × 8.1 Å) along the *b* axis (Fig. 1d). The pore spaces within the frameworks encapsulate a few disordered DMF solvent molecules. The potential solvent accessible void space accounts for approximately 42.5% of the whole crystal volume as estimated by PLATON.

With a slit rectangular channel along the *b* axis (3.8 Å × 8.1 Å), it is reasoned that 'slim' C_2H_4 molecules (3.28 Å × 4.18 Å × 4.84 Å) can access the channel in **HOF-4a** readily, while relatively 'fat' C_2H_6 molecules (3.81 Å × 4.08 Å × 4.82 Å) can hardly get through.[19] Furthermore, the amino groups residing on the surface wall of the framework might provide stronger hydrogen bonding interactions with more acidic C_2H_4 molecules (pK_a = 44) than C_2H_6 (pK_a = 50). We speculated that the size exclusion effect and hydrogen bonding interactions can work collaboratively to make **HOF-4** an ideal material to separate C_2H_4/C_2H_6. To test our hypothesis, gas adsorption experiments were conducted.

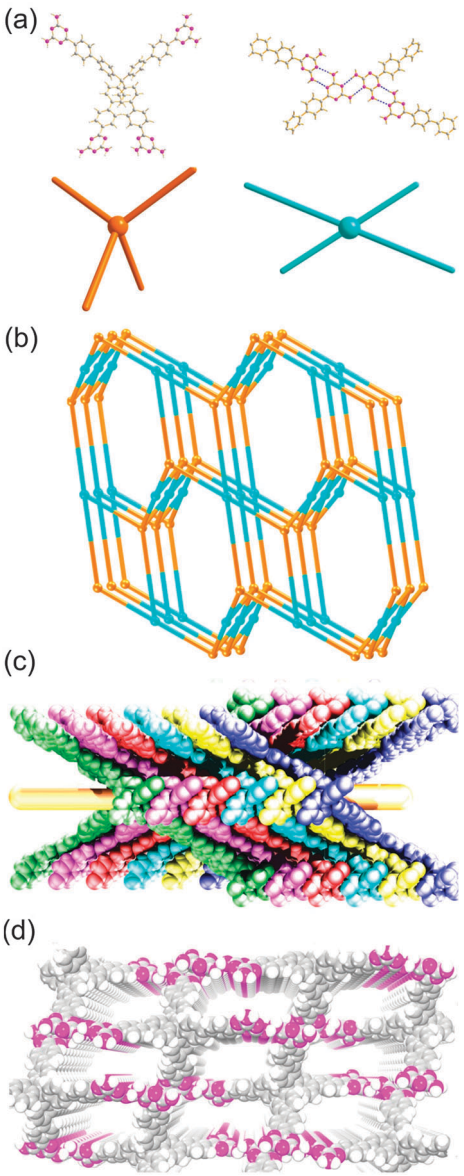

Fig. 1 X-ray structure of **HOF-4** featuring (a) the basic organic building block in which the central carbon atoms act as tetrahedral nodes (brown balls) and centres of multiple hydrogen bonding motifs act as square planar nodes (cyan balls); (b) a simplified binodal four-connected **PtS** $(4^2 8^4)$ topology; (c) six-fold interpenetrated frameworks; (d) the rectangular channels (3.8 × 8.1 Å) along the *b* axis (C, gray; H, white; N, pink).

Before examining adsorption properties, the guest solvent molecules in **HOF-4** were removed by solvent exchange with acetone and then vacuumed at 100 °C to obtain desolvated **HOF-4a** which is thermally stable up to 400 °C. The porosity of **HOF-4a** was evaluated by CO_2 gas sorption at 196 K (Fig. 2a). The type I isotherm shows a very sharp uptake at $P/P_0 < 0.1$, indicative of a microporous material. Because of the flexible nature of the HOF, there exists a small degree of sorption hysteresis. The isotherm gives an apparent Brunauer–Emmett–Teller (BET) surface area of 312 $m^2\ g^{-1}$ (Fig. S5, ESI†), which is moderate among a few examples of HOFs with permanent porosity.[15d]

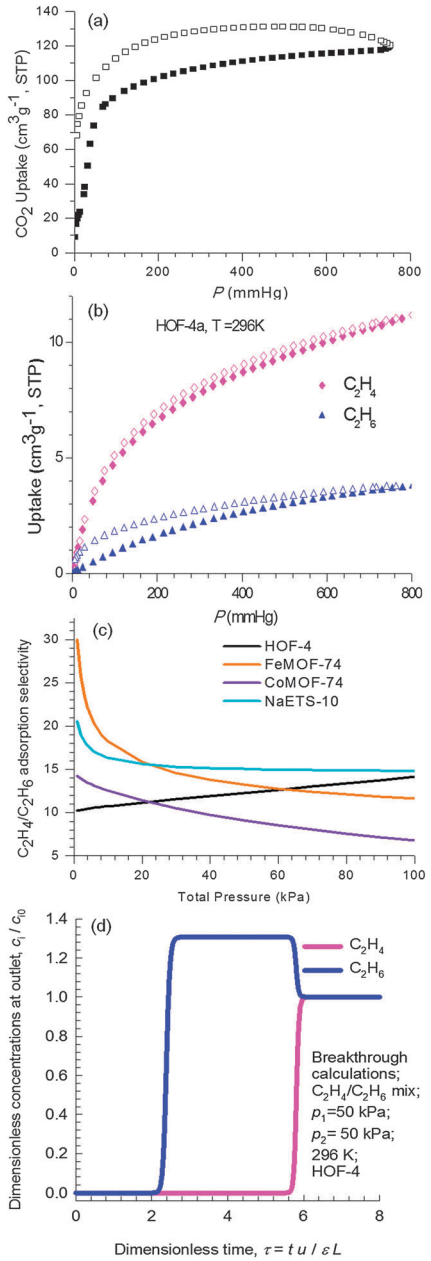

Fig. 2 (a) CO_2 sorption isotherm at 196 K; (b) single-component sorption isotherms for C_2H_4/C_2H_6 in **HOF-4a** at 296 K (solid symbol: adsorption, open symbol: desorption); (c) comparison of the IAST calculations of C_2H_4/C_2H_6 adsorption selectivities for **HOF-4**, FeMOF-74, CoMOF-74, and NaETS-10 at 296 K; (d) transient breakthrough of an equimolar C_2H_4–C_2H_6 mixture in an adsorber bed packed with **HOF-4** in the adsorption phase of a PSA operation. The inlet gas is maintained at partial pressures $p_1 = p_2 = 50$ kPa and at a temperature of 296 K.

Establishment of permanent microporosity in **HOF-4** allowed us to examine its utility as an adsorbent for industrially important C_2H_4/C_2H_6 separations. Interestingly, the C_2H_4 uptakes of 17.3 $cm^3\ g^{-1}$ at 273 K and 11.1 $cm^3\ g^{-1}$ at 296 K were systematically about three times higher than C_2H_6 uptakes of 5.1 $cm^3\ g^{-1}$ at 273 K and 3.6 $cm^3\ g^{-1}$ at 296 K at 1 atm (Fig. S6, ESI† and Fig. 2b). This discovery motivated us to examine its feasibility for the industrially important C_2H_4/C_2H_6 separation in more detail. The pure component isotherm data were fitted with the Langmuir isotherm model (Fig. S7, ESI†). To understand the binding energy at low coverage, isosteric heats of adsorption of C_2H_4 and C_2H_6 in **HOF-4a** were calculated. Fig. S8 (ESI†) presents data on the loading dependence of Q_{st} in **HOF-4a**. The binding energy for C_2H_4 in **HOF-4a** is 44 kJ mol^{-1}, which is comparable in magnitude to those of MgMOF-74 and CoMOF-74.[10g] In contrast, the binding energy for C_2H_6 in **HOF-4a** is only about 14 kJ mol^{-1}, indicating that the **HOF-4a**–C_2H_4 interaction is much stronger than **HOF-4a**–C_2H_6 interaction at low coverage. Because **HOF-4a** is quite flexible, so its pores can be slightly enlarged to accommodate a small amount of C_2H_6 during the adsorption process.

We further performed calculations using the ideal adsorbed solution theory (IAST) of Myers and Prausnitz.[20] Fig. 2c provides a comparison of the adsorption selectivity of C_2H_4–C_2H_6 in equimolar mixtures as a function of total bulk gas phase pressure in **HOF-4a** and three well-known porous materials (MOF materials: FeMOF-74[10a] and CoMOF-74;[10g] zeolite material: NaETS-10[8c]) at 296 K. It is worthy of note that the adsorption selectivity in respect of C_2H_4/C_2H_6 for **HOF-4a** is up to 14 at 1 atm and room temperature, which not only surpasses the selectivity of the best MOF materials but is also comparable to that of the best zeolite material NaETS-10 for such an important separation, highlighting **HOF-4a** as a promising material for C_2H_4/C_2H_6 separation for industrial usage. The large pore spaces enable both FeMOF-74 and CoMOF-74 to take up much more C_2H_6 with increasing pressure; while the narrow pore sizes in **HOF-4a** limit its adsorption capacity for C_2H_6 even under increasing pressure, so **HOF-4a** is unique for C_2H_4/C_2H_6 separation: the separation selectivity increases with increasing pressure.

In order to further validate the feasibility, breakthrough simulation experiments were carried out using the established methodology described in early publications of Krishna (see the ESI† for details).[20] The simulated breakthrough curves (Fig. 2d) clearly show that **HOF-4a** can efficiently separate C_2H_4 from the C_2H_4–C_2H_6 mixture at room temperature. The more poorly adsorbed saturated C_2H_6 breaks through earlier and can be recovered in a nearly pure form (Fig. S9, ESI†). During the adsorption cycle, C_2H_6 at purities $>99\%$ can be recovered for a certain duration. Once the entire bed is in equilibrium with the partial pressures $p_1 = p_2 = 50$ kPa, the desorption, or the "blowdown" cycle is initiated, by applying a vacuum or by purging with inert gas. 99.95% of ethylene can be recovered during the time interval, which can satisfy the purity requirement for production of ethylene as a feedstock in the polymer industry.

In summary, we have prepared and characterized a unique six-fold interpenetrated **HOF-4** material with **PtS** topology by using an expanded tetrahedral tecton **2**. The high degree of interpenetration not only enhanced the structural integrity but also appropriately tuned the channel size to make **HOF-4** an ideal adsorbent for C_2H_4/C_2H_6 separation. This is the first example of a porous hydrogen-bonded organic framework for such an important industrial hydrocarbon separation, during which the channel confinement effect and hydrogen bonding interactions appear to simultaneously control the uptake of different C2 hydrocarbons. It is believed that this work could

render a new strategy for designing robust HOFs with permanent porosity and promote more investigation on separation of small hydrocarbons using novel porous organic materials.

This work was supported by the awards from the Welch Foundation AX-1730.

Notes and references

‡ Crystal data for **HOF-4**: $C_{61}H_{48}N_{20}$, M = 1061.17, monoclinic, space group $P2_1/n$, a = 20.212(2) Å, b = 7.725(2) Å, c = 26.666(2) Å, β = 90.606(8)°, V = 3920.81(2) Å^3, Z = 2, D_c = 0.899 g cm^{-3}, T = 193(2) K, $F(000)$ = 1108.0, final R_1 = 0.0976 for $I > 2\sigma(I)$, wR_2 = 0.2139 for all data, GOF = 1.133, CCDC 1010353.

1 (*a*) M. Benali and B. Aydin, *Sep. Purif. Technol.*, 2010, **73**, 377–390; (*b*) S. Matar and L. F. Hatch, *Chemistry of Petrochemical Processes*, Gulf Publishing Company, Texas, 2nd edn, 2000.
2 S. U. Rege, J. Padin and R. T. Yang, *AIChE J.*, 1998, **44**, 799–809.
3 (*a*) R. B. Eldridge, *Ind. Eng. Chem. Res.*, 1993, **32**, 2208–2212; (*b*) T. Ren, M. Patel and K. Blok, *Energy*, 2006, **31**, 425–451.
4 (*a*) M. Teramoto, S. Shimizu, H. Matsuyama and N. Matsumiya, *Sep. Purif. Technol.*, 2005, **44**, 19–29; (*b*) K. Kuraoka, S. Matsuura and K. Ueda, *Chem. Lett.*, 2014, **43**, 582–583; (*c*) M. Takht Ravanchi, T. Kaghazchi and A. Kargari, *Desalination*, 2009, **235**, 199–244.
5 (*a*) L. C. Tome, D. Mecerreyes, C. S. R. Freire, L. P. N. Rebelo and I. M. Marrucho, *J. Mater. Chem. A*, 2014, **2**, 5631–5639; (*b*) L. Moura, M. Mishra, V. Bernales, P. Fuentealba, A. A. H. Padua, C. C. Santini and M. F. Costa Gomes, *J. Phys. Chem. B*, 2013, **117**, 7416–7425; (*c*) N. Ghasem, M. Al-Marzouqi and Z. Ismail, *Sep. Purif. Technol.*, 2014, **127**, 140–148.
6 A. van Miltenburg, W. Zhu, F. Kapteijn and J. A. Moulijn, *Chem. Eng. Res. Des.*, 2006, **84**, 350–354.
7 A. C. Dewitt, K. W. Herwig and S. Lombardo, *Adsorption*, 2005, **11**, 491–499.
8 (*a*) M. Mofarahi and S. M. Salehi, *Adsorption*, 2013, **19**, 101–110; (*b*) M. Shi, A. M. Avila, F. Yang, T. M. Kuznicki and S. M. Kuznicki, *Chem. Eng. Sci.*, 2011, **66**, 2817–2822; (*c*) A. Anson, Y. Wang, C. C. H. Lin, T. M. Kuznicki and S. M. Kuznicki, *Chem. Eng. Sci.*, 2008, **63**, 4171–4175.
9 L. Huang and D. Cao, *J. Mater. Chem. A*, 2013, **1**, 9433–9439.
10 (*a*) E. D. Bloch, W. L. Queen, R. Krishna, J. M. Zadrozny, C. M. Brown and J. R. Long, *Science*, 2012, **335**, 1606; (*b*) Y.-S. Bae, C. Y. Lee, K. C. Kim, O. K. Farha, P. Nickias, J. T. Hupp, S. T. Nguyen and R. Q. Snurr, *Angew. Chem., Int. Ed.*, 2012, **51**, 1857–1860; (*c*) J. R. Li, R. J. Kuppler and H. C. Zhou, *Chem. Soc. Rev.*, 2009, **38**, 1477–1504; (*d*) C. Gucuyener, J. van den Bergh, J. Gascon and F. Kapteijn, *J. Am. Chem. Soc.*, 2010, **132**, 17704–17706; (*e*) K. Li, D. H. Olson, J. Seidel, T. J. Emge, H. Gong, H. Zeng and J. Li, *J. Am. Chem. Soc.*, 2009, **131**, 10368–10369; (*f*) C. Yu, M. G. Cowan, R. D. Noble and W. Zhang, *Chem. Commun.*, 2014, **50**, 5745–5747; (*g*) Y. He, R. Krishna and B. Chen, *Energy Environ. Sci.*, 2012, **5**, 9107–9120; (*h*) H. L. Jiang and Q. Xu, *Chem. Commun.*, 2011, **47**, 3351–3370.
11 G. G. Chang, Z. B. Bao, Q. L. Ren, S. G. Deng, Z. G. Zhang, B. G. Su, H. B. Xing and Y. W. Yang, *RSC Adv.*, 2014, **4**, 20230–20233.
12 (*a*) B. Li, Y. Zhang, R. Krishna, K. Yao, Y. Han, Z. Wu, D. Ma, Z. Shi, T. Pham, B. Space, J. Liu, P. K. Thallapally, J. Liu, M. Chrzanowski and S. Ma, *J. Am. Chem. Soc.*, 2014, **136**, 8654–8660; (*b*) M. H. Weston, Y. J. Colon, Y.-S. Bae, S. J. Garibay, R. Q. Snurr, O. K. Farha, J. T. Hupp and S. T. Nguyen, *J. Mater. Chem. A*, 2014, **2**, 299–302; (*c*) W. Lu, D. Yuan, D. Zhao, C. I. Schilling, O. Plietzsch, T. Muller, S. Bräse, J. Guenther, J. Blümel, R. Krishna, Z. Li and H.-C. Zhou, *Chem. Mater.*, 2010, **22**, 5964–5972.
13 W. Zhu, J. C. Groen, A. v. Miltenburg, F. Kapteijn and J. A. Moulijn, *Carbon*, 2005, **43**, 1416–1423.
14 X. Tian, Z. Wang, Z. Yang, P. Xiu and B. Zhou, *J. Phys. D: Appl. Phys.*, 2013, **46**, 395302.
15 (*a*) K. E. Maly, E. Gagnon, T. Maris and J. D. Wuest, *J. Am. Chem. Soc.*, 2007, **129**, 4306; (*b*) J. D. Wuest, *Chem. Commun.*, 2005, 5830; (*c*) J. Tian, P. K. Thallapally and B. P. McGrail, *CrystEngComm*, 2012, **14**, 1909–1919; (*d*) M. Mastalerz, *Chem. – Eur. J.*, 2012, **18**, 10082–10091; (*e*) P. S. Nugent, V. L. Rhodus, T. Pham, K. Forrest, L. Wojtas, B. Space and M. J. Zaworotko, *J. Am. Chem. Soc.*, 2013, **135**, 10950; (*f*) X.-Z. Luo, X.-J. Jia, J.-H. Deng, J.-L. Zhong, H.-J. Liu, K.-J. Wang and D.-C. Zhong, *J. Am. Chem. Soc.*, 2013, **135**, 11684; (*g*) P. Li, Y. He, J. Guang, L. Weng, J. C.-G. Zhao, S. Xiang and B. Chen, *J. Am. Chem. Soc.*, 2014, **136**, 547; (*h*) Y. He, S. Xiang and B. Chen, *J. Am. Chem. Soc.*, 2011, **133**, 14570; (*i*) M. Mastalerz and I. M. Oppel, *Angew. Chem., Int. Ed.*, 2012, **51**, 5252; (*j*) S. Dalapati, R. Saha, S. Jana, A. K. Patra, A. Bhaumik, S. Kumar and N. Guchhait, *Angew. Chem., Int. Ed.*, 2012, **51**, 12534–12537.
16 B. Chen, M. Eddaoudi, S. T. Hyde, M. O'Keeffe and O. M. Yaghi, *Science*, 2001, **291**, 1021–1023.
17 S. B. Choi, H. Furukawa, H. J. Nam, D. Y. Jung, Y. H. Jhon, A. Walton, D. Book, M. O'Keeffe, O. M. Yaghi and J. Kim, *Angew. Chem., Int. Ed.*, 2012, **51**, 8791–8795.
18 X. L. Wang, C. Qin, E. B. Wang, Y. G. Li and Z. M. Su, *Chem. Commun.*, 2005, 5450–5452.
19 C. E. Webster, R. S. Drago and M. C. Zerner, *J. Am. Chem. Soc.*, 1998, **120**, 5509–5516.
20 (*a*) A. L. Myers and J. M. Prausnitz, *AIChE J.*, 1965, **11**, 121; (*b*) R. Krishna and J. R. Long, *J. Phys. Chem. C*, 2011, **115**, 12941; (*c*) R. Krishna, *Microporous Mesoporous Mater.*, 2014, **185**, 30; (*d*) R. Krishna and R. Baur, *Sep. Purif. Technol.*, 2003, **33**, 213.

Supporting Information

A microporous six-fold interpenetrated hydrogen-bonded organic framework with for highly selective separation of C_2H_4/C_2H_6

Peng Li,[a] Yabing He,[a] Hadi D. Arman,[a] Rajamani Krishna,[b] Hailong Wang,[a] Linhong Weng,[c] Banglin Chen*[a,d]

[a] *Department of Chemistry, University of Texas at San Antonio, One UTSA Circle, San Antonio, Texas 78249-0698, United States Fax: (+1)-210-458-7428; E-mail: banglin.chen@utsa.edu*

[b] *Van 't Hoff Institute for Molecular Sciences, University of Amsterdam, Science Park 904, 1098 XH Amsterdam, The Netherlands*

[c] *Department of Chemistry, Fudan University, Shanghai, 200433, People's Republic of China.*

[d] *Department of Chemistry, Faculty of Science, King Abdulaziz University, Jeddah 22254, Saudi Arabia*

1. General remark

Thermogravimetric analyses (TGA) were performed with a Shimadzu TGA-50 analyzer under nitrogen atmosphere with a heating rate of 3 ^{o}C min^{-1}. Powder X-ray diffraction (PXRD) patterns were recorded by a Rigaku Ultima IV diffractometer operated at 40 kV and 44 mA with a scan rate of 1.0 deg min^{-1}. FTIR spectra were performed at a Bruke Vector 22 infrared spectrometer at room temperature. ^{1}H NMR and ^{13}C NMR spectra were obtained using a Varian Mercury 300 MHz spectrometer at room temperature. Tetramethylsilane (TMS) and deuterated solvents ($CDCl_3$, δ = 77.0 ppm; DMSO-d_6, δ = 39.5 ppm) were used as internal standards in ^{1}H NMR and ^{13}C NMR experiments, respectively. The elemental analyses were performed with Perkin–Elmer 240 CHN analyzers from Galbraith Laboratories, Knoxville. A Micromeritics ASAP 2020 surface area analyzer was used to measure gas adsorption isotherms. To have a guest-free framework, the fresh sample was exchanged with diethyl ether for at least 3 times, filtered and dried at room temperature for 24 hrs prior to measurements. The crystallographic measurement was performed on a Rigaku X-ray diffractometer system equipped with a Mo-target X-ray tube (λ = 0.71073 Å) at 193 (2) K. The structure was solved by direct methods and refined by full matrix least-squares methods with the SHELX-97 program package. The solvent molecules in as-synthesized HOF crystal are in highly disordered. The SQUEEZE subroutine of the PLATON software suit was used to remove the scattering from the highly disordered guest molecules.

2. General procedure of synthesis of organic building block and HOF-4

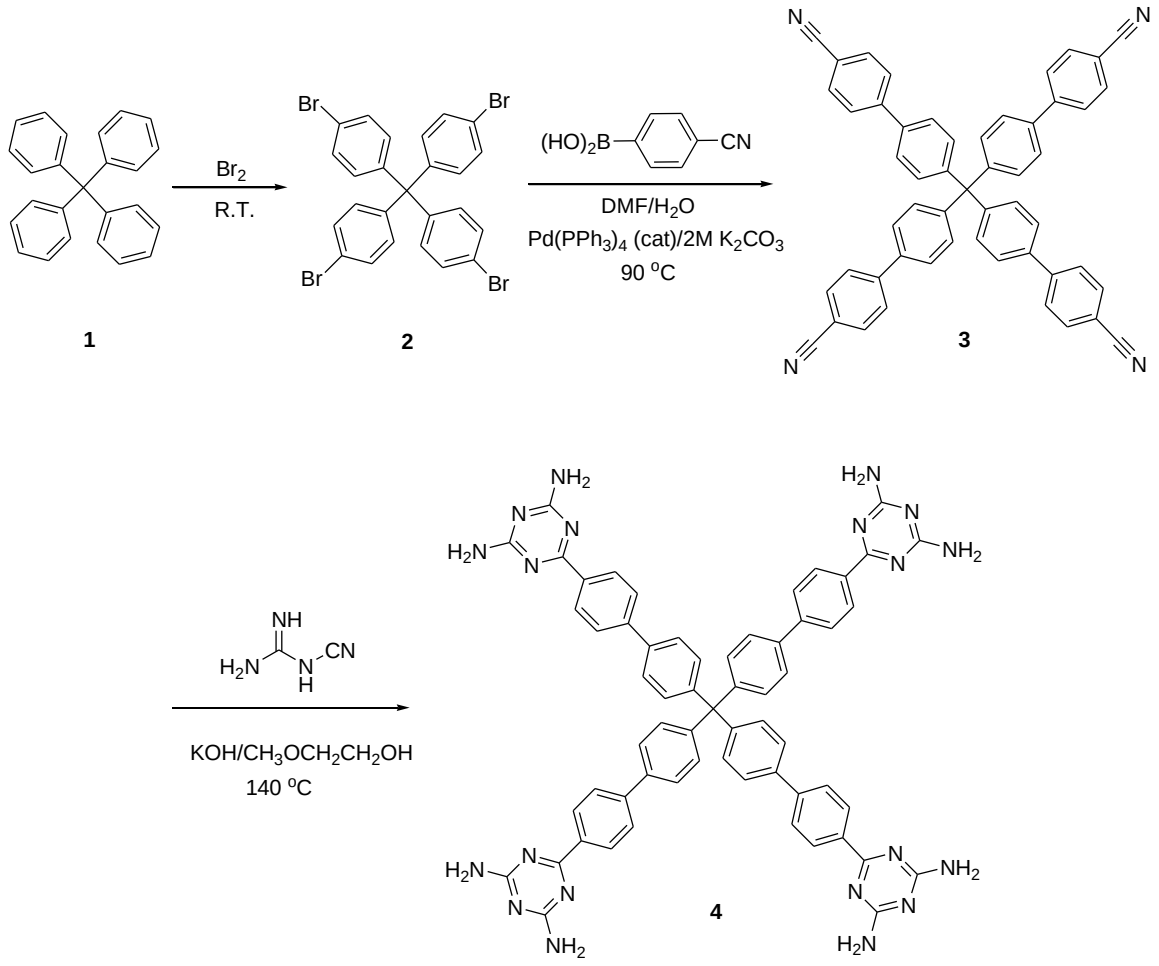

Scheme S1. Synthesis and characterization of the organic building block **4**

Tetrakis(4-bromophenyl)methane (2): Bromine (10.00 mL, 194.61 mmol) was added slowly to tetraphenylmethane (**1**) (9.00 g, 28.09 mmol) with continuous stirring. The resulting slurry was stirred for an additional 5 h and then poured into ethanol (200 mL) which was cooled to -78 ^{o}C. The precipitated solid was filtered, washed with saturated aqueous NaHSO3 solution (80 mL 3) and dried at 60 oC under vacuum to give a white solid (17.52 g, 27.55 mmol) in 98% yield. ^{1}H NMR (DMSO-*d*6, 300.0 MHz) δ (ppm): 7.51 (d, J = 8.7 Hz, 8H), 6.99 (d, J = 8.7 Hz, 8H); ^{13}C

NMR (DMSO-*d*6, 75.4 MHz) δ (ppm): 144.34, 132.20, 130.93, 119.81, 63.17; FTIR (neat, cm^{-1}): 1569, 1479, 1079, 1009, 950, 914, 835, 810, 752, 729, 679.

Tetrakis(4'-cyano-[1,1'-biphenyl]-4-yl)methane (3): A mixture of 4-cyanophenylboronic acid (17.63 g, 120.01 mmol) and tetrakis(4-bromophenyl)methane (13.63 g, 21.43 mmol) in DMF (80 mL), H_2O (40 mL), and aqueous K_2CO_3 (40 mL, 2M) was degassed by allowing N_2 to bubble through it. $Pd(PPh_3)_4$ (1150 mg, 1.00 mmol) was then added, and the mixture was degassed again. The mixture was heated at 90 ^oC for 48 h under N_2 and was exposed to air for 1 h to oxidize the catalyst. After removal of solvent under vacumn, the residue was extracted with CH_2Cl_2 (100 mL×3) and aqueous sodium ethylenediaminetetraacetate (50 mL×3) and brine (50 mL). The organic layer was separated and dried over anhydrous magnesium sulfate, filtered and evaporated to dryness. The resulting residue was purified by silica gel column chromatography with $CHCl_3$ as eluent to give a white solid (8.99 g, 12.42 mmol) in 58% yield. ^1H NMR (CDCl3, 300.0 MHz) δ (ppm): δ 7.72 (d, *J* = 5.4 Hz, 4H), 7.55 (d, *J* = 5.7 Hz, 2H), 7.44 (s, 2H).

Tetrakis(4'-(2,4-diamino-1,3,5-triazin-6-yl)-[1,1'-biphenyl]-4-yl)methane (4): a mixture of Tetrakis(4'-cyano-[1,1'-biphenyl]-4-yl)methane (3.75 g, 5.18 mmol), dicyandiamide (2.18 g, 25.93 mmol) and KOH (85%, 0.32 g, 4.85 mmol) in methyl cellosolve (25 mL) was stirred at 140 ^oC for 24 h under nitrogen atmosphere. The mixture was then cooled to room temperature and poured into methanol (125 mL). The precipitated solid was filtered, washed with boiling water and methanol, respectively, and dried under vacuum at 90 ^oC to give a white solid (5.05 g, 4.76 mmol) in 92% yield. ^1H NMR (500 MHz, DMSO-d_6) δ (ppm): 8.31 (d, *J* = 7.6 Hz, 2H), 7.78 (dd, *J* = 15.1, 7.7 Hz, 4H), 7.41 (d, *J* = 7.3 Hz, 2H), 6.76 (s, 4H); ^{13}C NMR (500 MHz, DMSO-d_6) δ (ppm): 170.29, 167.87, 146.35, 142.28, 137.58, 136.63, 131.49, 128.78, 126.78, 109.74, 64.36. FTIR (neat, cm^{-1}): 3607, 3469, 3320, 3172, 1599, 1511, 1427, 1381, 1240, 992, 808.

3. Crystallization of the compound HOF-4

Compound **4** (200 mg, 0.189 mmol) was dissolved in DMF (20 mL) under heating. The resulting solution was cooled to room temperature and filtered. The filtrate was divided to 8 small disposable scintillation vials. These vials were allowed to sit and evaporate at room temperature for a week. Colorless needle-like crystals were obtained in 79% yield.

4. Fitting of pure component isotherms

The measured experimental isotherm data for C_2H_4 on HOF-4 were fitted with the dual-Langmuir isotherm model

$$q = q_{A,sat}\frac{b_A p}{1+b_A p} + q_{B,sat}\frac{b_B p}{1+b_B p} \tag{1}$$

with *T*-dependent parameters

$$b_A = b_{A0}\exp\left(\frac{E_A}{RT}\right); \quad b_B = b_{B0}\exp\left(\frac{E_B}{RT}\right)$$

For the pure component isotherms of C_2H_6, a simpler single-site Langmuir model is of adequate accuracy. The fit parameters for both components are specified in Table S2. Figure S7 presents a comparison of the experimentally determined component loadings for C_2H_4, on HOF-4 at 296 K with the isotherm fits using parameters specified in Table S2. The fits are excellent over the entire range of pressures (Note: HOF-4a adsorbs the unsaturated C_2H_4 in preference to the saturated C_2H_6. When all the strong adsorption sites are occupied, further adsorption of C_2H_4 is only possible at weaker sites. Consequently, the isotherms of C_2H_4 exhibit an inflection. To describe such inflection we need a 2-site Langmuir fit. C_2H_6 isotherms do not exhibit any inflection and so a single site Langmuir isotherm is of sufficient accuracy).

5. Calculations of adsorption selectivity

The selectivity of preferential adsorption of component 1 over component 2 in a mixture containing 1 and 2, can be formally defined as

$$S_{ads} = \frac{q_1/q_2}{p_1/p_2} \tag{2}$$

In equation (2), q_1 and q_2 are the component loadings of the adsorbed phase in the mixture. The calculations of S_{ads} are based on the use of the Ideal Adsorbed Solution Theory (IAST) of Myers and Prausnitz.[1]

Based on the IAST calculations for C_2H_4/C_2H_6 adsorption selectivities in HOF-4, at a total pressure of 100 kPa, the value of S_{ads} for HOF-4 is 14. This value is higher than that for MgMOF-74, CoMOF-74, and CuBTC.[2]

6. Isosteric heats of adsorption

The isosteric heat of adsorption, Q_{st}, were calculated using the Clausius-Clapeyron equation by differentiation of the dual-Langmuir fits of the isotherms.

Figure S8 compares the isosteric heats of adsorption, Q_{st}, for C_2H_4 and C_2H_6 in HOF-4. The binding energy for C_2H_4 in HOF-4 is 44 kJ mol^{-1} ; this value is comparable in magnitude to that of MgMOF-74, and CoMOF-74. [2]

7. Simulations of C_2H_4/C_2H_6 breakthroughs in packed beds

Transient breakthrough simulations were carried out using the simulation methodology described in the literature.[3, 4] For the breakthrough simulations, the following parameter values were used: framework density, ρ= 899 kg m^{-3}, length of packed bed, L = 0.12 m; voidage of packed bed, ε= 0.75; superficial gas velocity at inlet, u = 0.00225 m/s. The transient breakthrough are presented in our investigation in terms of a *dimensionless* time, τ, defined by dividing the actual time, t, by the characteristic time, $\frac{L\varepsilon}{u_0}$.

Let us first consider the adsorption phase of the PSA operations. Figure 2d shows transient breakthrough of an equimolar C_2H_4/C_2H_6 mixture in an adsorber bed packed with HOF-4. The inlet gas is maintained at partial pressures $p_1 = p_2 = 50$ kPa. The more poorly adsorbed saturated C_2H_6 breaks through earlier and can be recovered in nearly pure form. From the gas phase concentrations at the exit of the adsorber, we can determine the % C_2H_6; this information is presented in Figure S9. During the adsorption cycle, C_2H_6 at purities > 99% can be recovered for a certain duration of the adsorption cycle.

Once the entire bed is in equilibrium with the partial pressures $p_1 = p_2 = 50$ kPa, the desorption, or "blowdown" cycle is initiated, by applying a vacuum or purging with inert gas. Figure S9b shows % C_2H_4 in the outlet gas of an adsorber bed packed with HOF-4 in the desorption cycle. For production of ethene as feedstock for polymerization purposes, the required purity level is 99.95%+ can be recovered during the time interval indicated by the arrow in Figure S9a.

Notation

b_A	dual-Langmuir constant for species *i* at adsorption site A, Pa^{-1}
b_B	dual-Langmuir constant for species *i* at adsorption site B, Pa^{-1_i}
c_i	molar concentration of species *i* in gas mixture, mol m^{-3}
c_{i0}	molar concentration of species *i* in gas mixture at inlet to adsorber, mol m^{-3}
L	length of packed bed adsorber, m
p_i	partial pressure of species *i* in mixture, Pa
p_t	total system pressure, Pa
q_i	component molar loading of species *i*, mol kg^{-1}
$q_{sat,A}$	saturation loading of site A, mol kg^{-1}
$q_{sat,B}$	saturation loading of site B, mol kg^{-1}
S_{ads}	adsorption selectivity, dimensionless
t	time, s
T	absolute temperature, K
u	superficial gas velocity in packed bed, m s^{-1}

Greek letters

	voidage of packed bed, dimensionless
	framework density, kg m^{-3}
	time, dimensionless

Subscripts

i	referring to component *i*
A	referring to site A
B	referring to site B

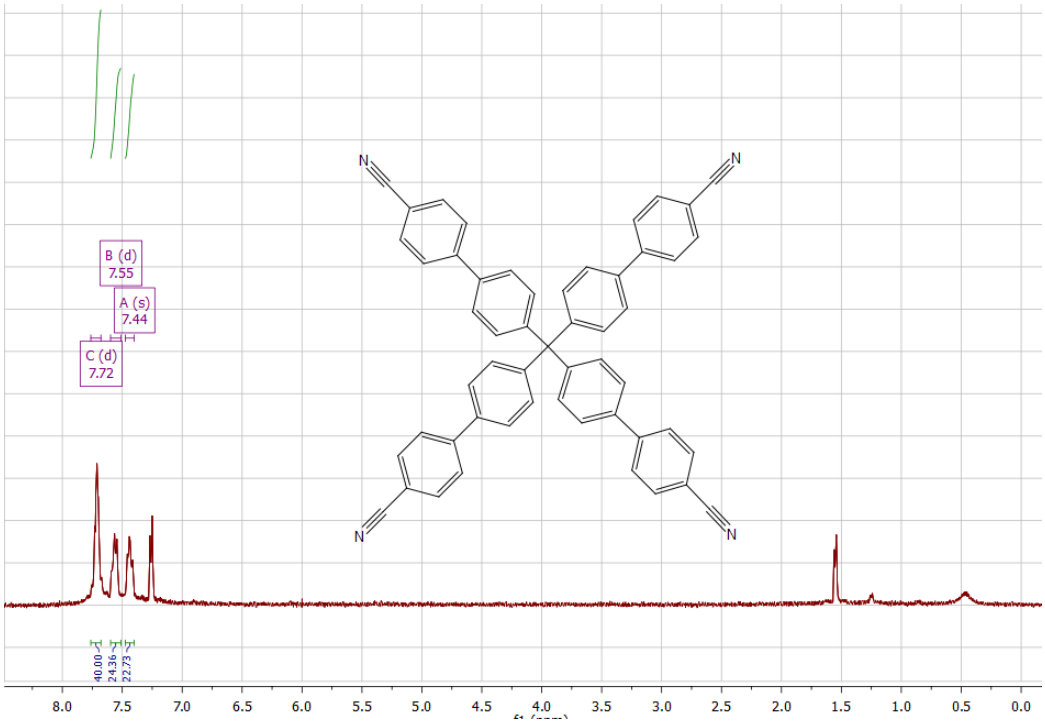

Figure S0. ^{1}H NMR spectra of the organic building block **3**.

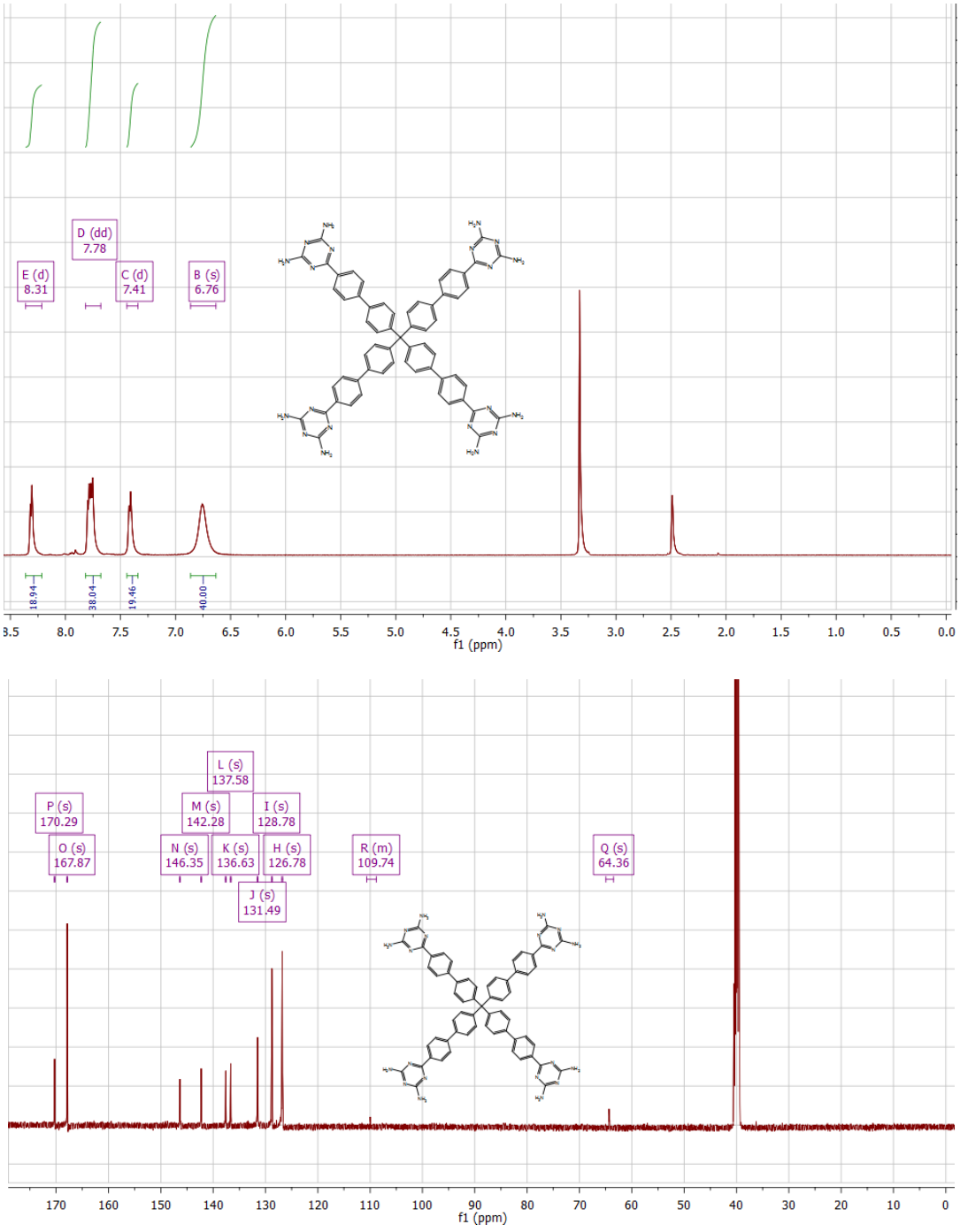

Figure S1. ^{1}H NMR (top) and ^{13}C NMR (bottom) spectra of the activated organic building block **4**.

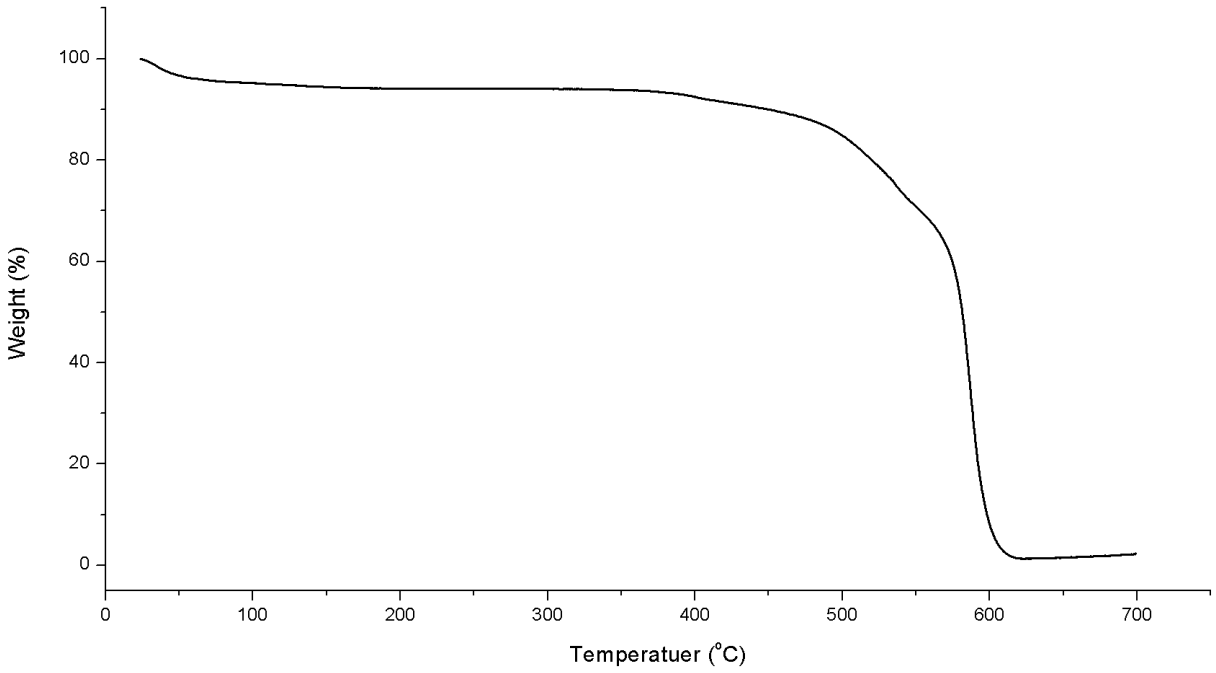

Figure S2. TGA curve of **HOF-4a**.

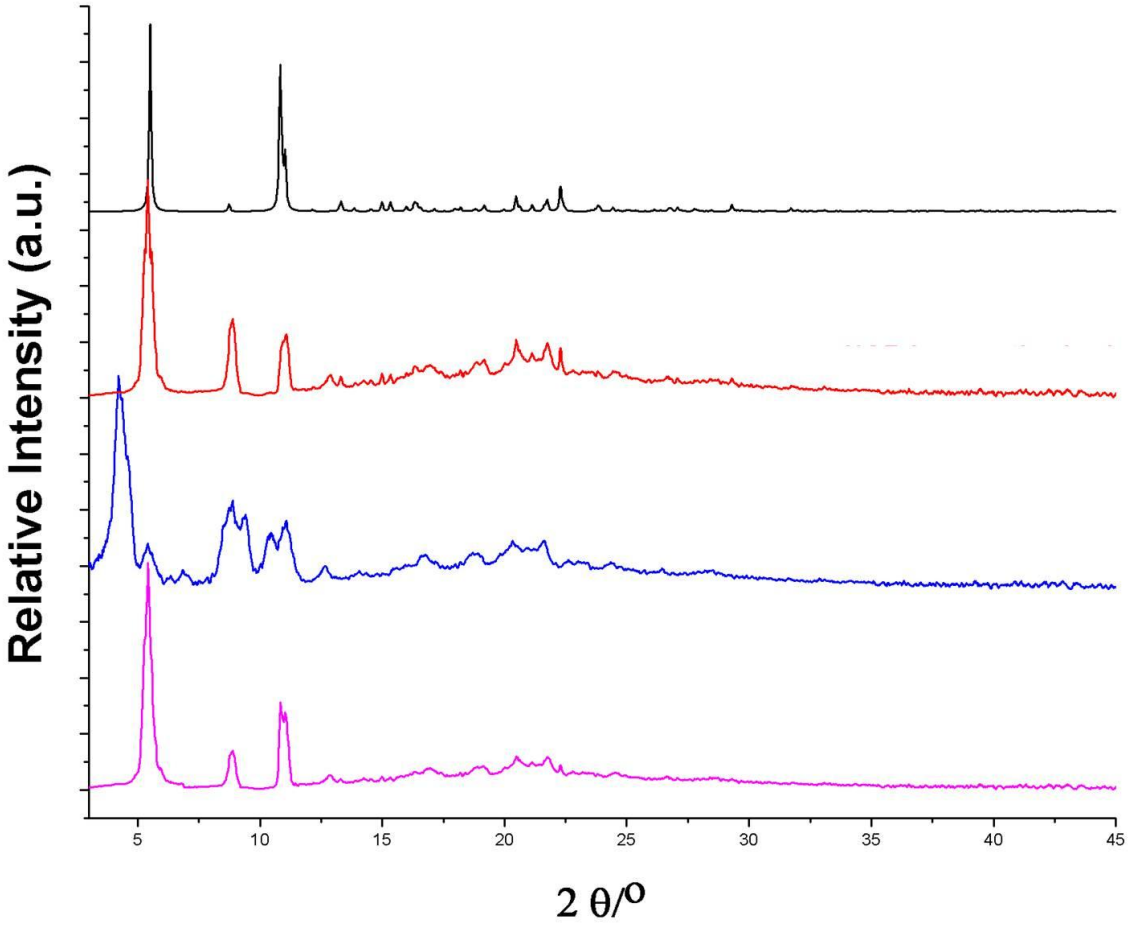

Figure S3. PXRD of simulated **HOF-4** (black), as-synthesized **HOF-4** (red), **HOF-4a** (blue) , and regenerated **HOF-4** (pink)**.**

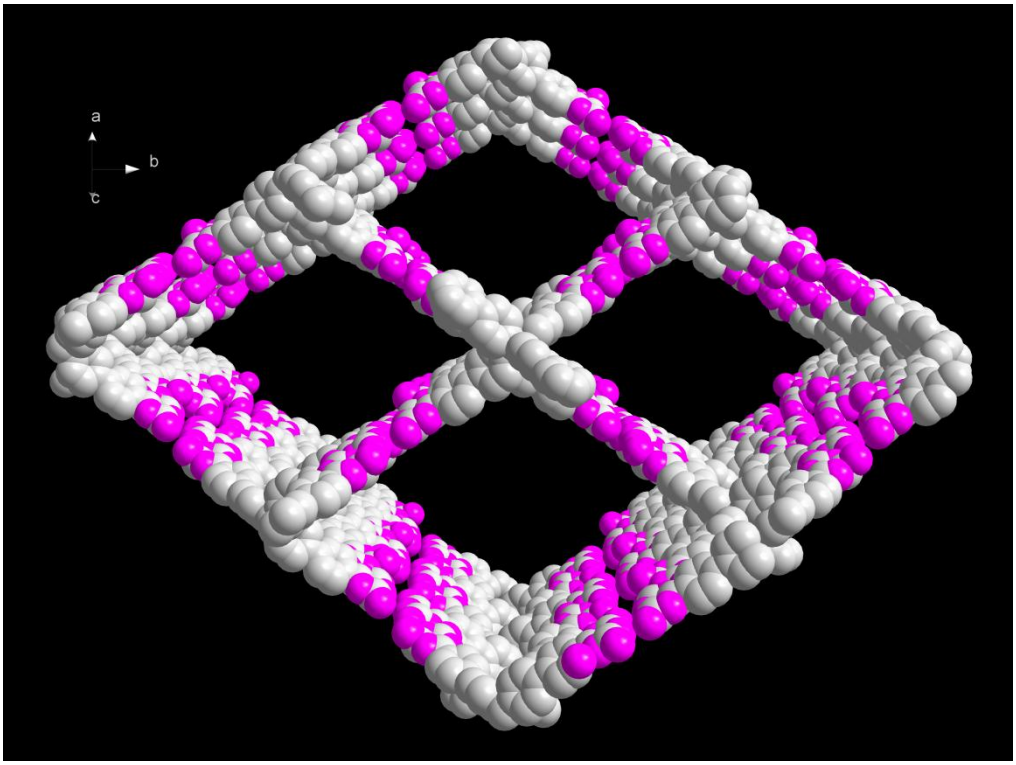

Figure S4. Rhombic channels in the single net of **HOF-4** along [101] direction with an approximate dimension of *c.a.* 40 Å × 30 Å along the diagonals

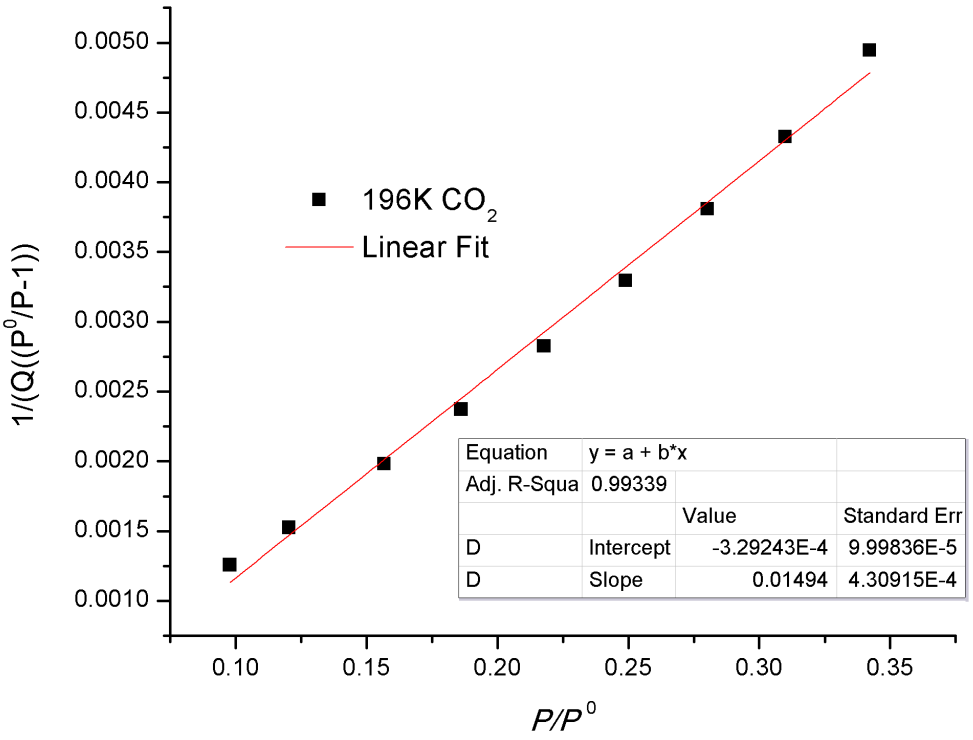

S_{BET} = (1/(-0.00033+0.01494)) / 22414 × 6.023 × 10^{23} × 0.170 × 10^{-18} = 312.67 m^2g^{-1}

Figure S5. CO_2 adsorption isotherm at 196 K (a) and the BET surface areas of **HOF-4a** (b).

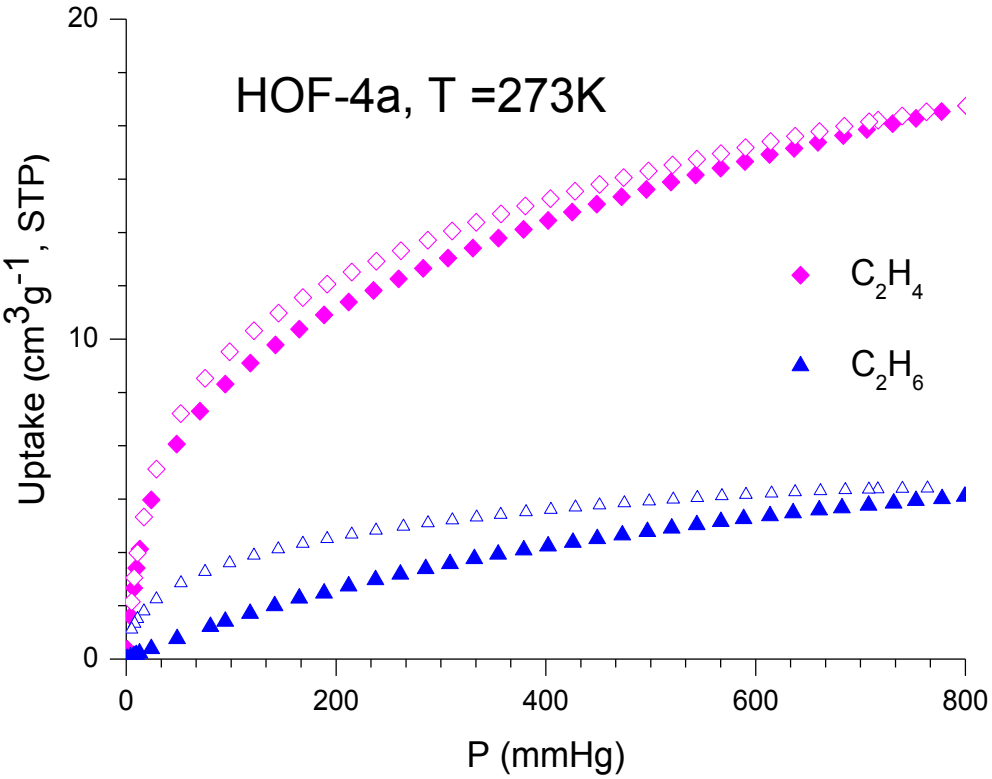

Figure S6. Single-component sorption isotherms for C_2H_4/C_2H_6 in **HOF-4a** at 273 K (Solid symbol: adsorption, open symbol: desorption).

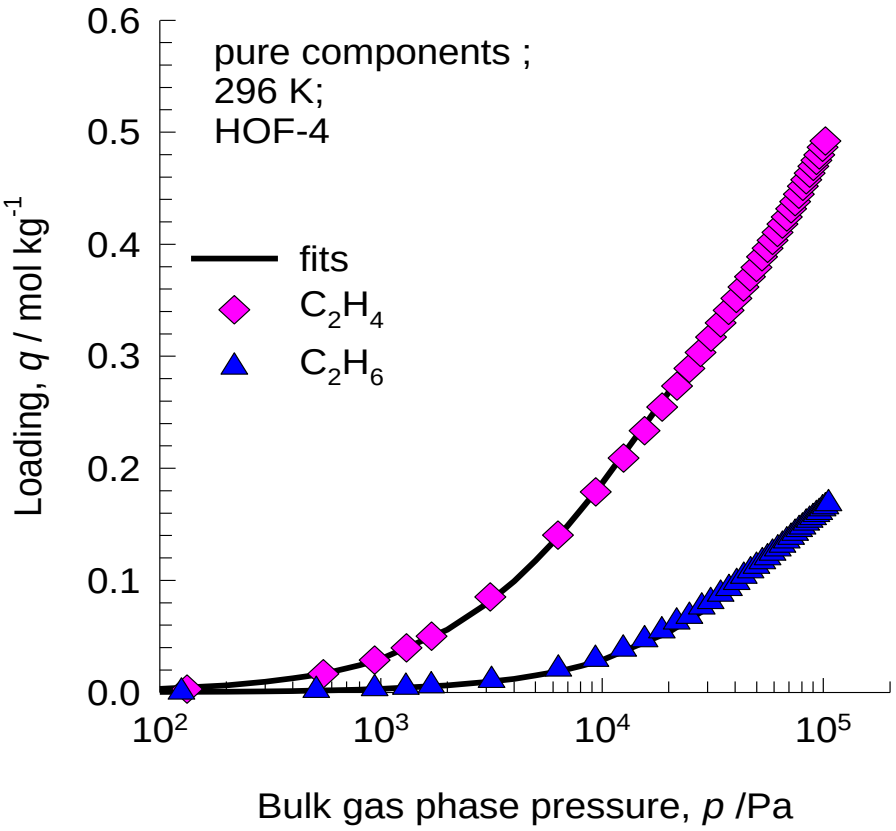

Figure S7. Comparison of the experimentally determined component loadings for C_2H_4, and C_2H_6 in HOF-4 at 296 K with the isotherm fits using parameters specified in Table S2.

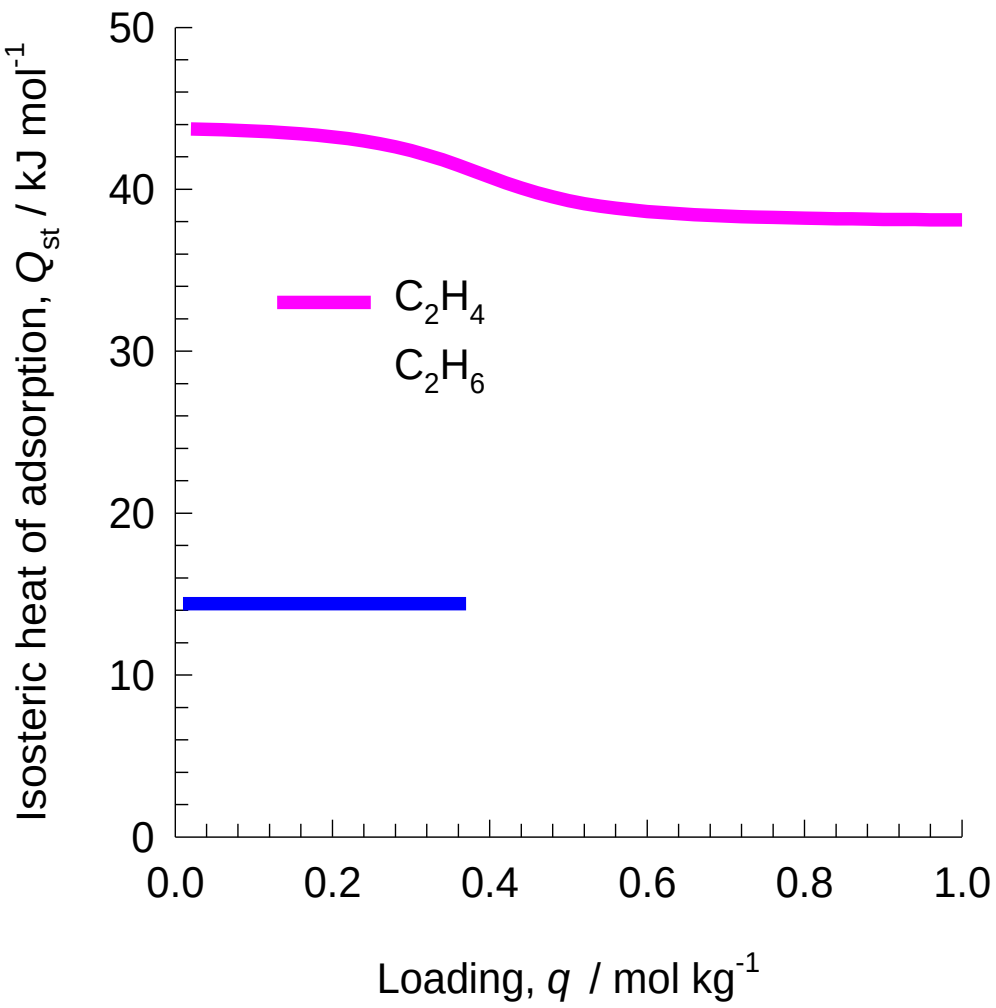

Figure S8. Comparison of the isosteric heats of adsorption, Q_{st}, for C_2H_4, and C_2H_6 in HOF-4.

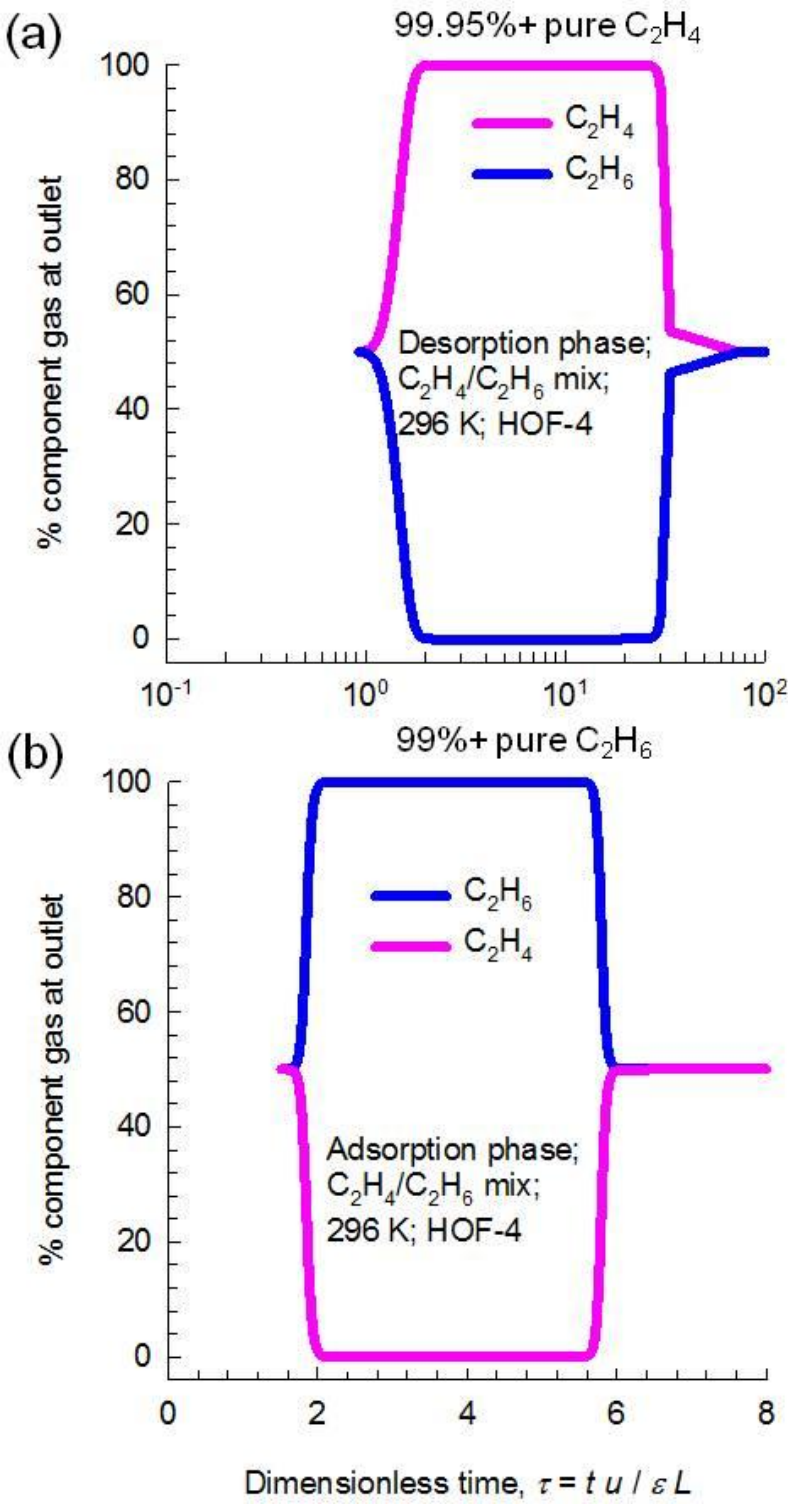

Figure S9. % C_2H_4 and % C_2H_6 in the outlet gas of an adsorber bed packed with HOF-4 in the (a) desorption cycle and (b) adsorption cycle. The inlet gas is maintained at partial pressures $p_1 = p_2$ = 50 kPa, at a temperature of 296 K.

Table S1. Geometry of hydrogen-bonds linked together by adjacent four building blocks in **HOF-4**

D-H…*A*	*D*…H	H…*A*	*D*…*A*	*D*-H…*A*
N5-H5A…N13[i]	0.86	2.1870 (2)	3.0285	166
N10-H10A…N16[ii]	0.86	2.1285(5)	2.9798	170
N14-H14A…N17[iii]	0.86	2.1730(4)	3.0212	169
N15-H15B…N1[ii]	0.86	2.2041(4)	3.0638	179
N19-H19A…N7[i]	0.86	2.1510(4)	2.9390	152
N20-H20A…N12[iv]	0.86	2.0853(4)	2.9407	173

Symmetry codes: (i) = 1/2+x,1-y,1/2+z; (ii) = -1/2+x,1-y,-1/2+z; (iii) = 1/2+x,4-y,-1/2+z;

(iv) = -1/2+x,4-y,1/2+z;

Table S2. Dual-Langmuir fits for C_2H_4, and C_2H_6 in HOF-4. For both components, the fits are based on the adsorption branch of the isotherms.

	Site A			Site B		
	$q_{A,sat}$ mol kg^{-1}	b_{A0} Pa^{-1}	E_A kJ mol^{-1}	$q_{B,sat}$ mol kg^{-1}	b_{B0} Pa^{-1}	E_B kJ mol^{-1}
C_2H_4	2	1.28×10^{-13}	38	0.4	1.32×10^{-12}	44
C_2H_6	0.38	2.37×10^{-8}	14.4			

Table S3. Crystal data and structure refinement for **HOF-4**

Identification code	**HOF-4**
Empirical formula	$C_{61}H_{48}N_{20}$
Formula weight	1061.19
Temperature (K)	193(2)
Crystal system	Monoclinic
Space group	*P*2/n
a (Å)	20.212(6)
b (Å)	7.275(2)
c (Å)	26.666(8)
α (°)	90.00
β (°)	90.606(6)
γ (°)	90.00
Volume ($Å^3$)	3921(2)
Z	2
Calculated density (g/cm^3)	0.899
Adsorption coefficient (mm^{-1})	0.057
F(000)	1108.0
Crystal size (mm)	0.4 × 0.07 × 0.05
Radiation	MoKα (λ = 0.71073)
Theta range for data collection	4.98 to 50.02 °
Index ranges	$-24 \le h \le 24$, $-8 \le k \le 7$, $-31 \le l \le 31$
Reflections collected	20646
Independent reflections	6927 [R_{int} = 0.0549, R_{sigma} = 0.0570]
Data/restraints/parameters	6927/0/393
Goodness-of-fit on F^2	1.133
Final R indexes [$I >= 2\sigma(I)$]	R_1 = 0.0976, wR_2 = 0.1992
Final R indexes [all data]	R_1 = 0.1442, wR_2 = 0.2139
Largest diff. peak/hole (e. $Å^{-3}$)	0.50/-0.42
CCDC No.	1010353

8. References

[1] A. L. Myers and J. M. Prausnitz, *A.I.Ch.E.J.*, 1965, **11**, 121-130.

[2] Y. He, R. Krishna, B. Chen, *Energy Environ. Sci.*, 2012**, 5**, 9107.

[3] R. Krishna and J. R. Long, *J. Phys. Chem. C*, 2011, **115**, 12941-12950.

[4] R. Krishna, *Microporous Mesoporous Mater.*, 2014, **185**, 30-50.